Supporting Information

Unraveling the Bonding Complexity of Polyhalogen Anions: High-Pressure Synthesis of Unpredicted Sodium Chlorides Na_2Cl_3, Na_4Cl_5 and Bromide Na_4Br_5

Yuqing Yin[1,2*], Alena Aslandukova[3], Nityasagar Jena[4], Florian Trybel[4], Igor A. Abrikosov[4], Bjoern Winkler[5], Saiana Khandarkhaeva[3], Timofey Fedotenko[6], Elena Bykova[3,7], Dominique Laniel[8], Maxim Bykov[9], Andrey Aslandukov[1,3], Fariia I. Akbar[1,3], Konstantin Glazyrin[6], Gaston Garbarino[10], Carlotta Giacobbe[10], Eleanor L. Bright[10], Zhitai Jia[2], Leonid Dubrovinsky[3], Natalia Dubrovinskaia[1,4]

[1]Material Physics and Technology at Extreme Conditions, Laboratory of Crystallography, University of Bayreuth, 95440 Bayreuth, Germany
[2]State Key Laboratory of Crystal Materials, Shandong University, Jinan 250100, China
[3]Bayerisches Geoinstitut, University of Bayreuth, 95440 Bayreuth, Germany
[4]Department of Physics, Chemistry and Biology (IFM), Linköping University, SE-581 83, Linköping, Sweden
[5]Institute für Geowissenschaften, Frankfurt University, Altenhöferallee 1, DE-60438 Frankfurt am Main, Germany
[6]Deutsches Elektronen-Synchrotron DESY, Notkestr. 85, 22607 Hamburg, Germany
[7]Earth and Planets Laboratory, Carnegie Institution for Science, 5241 Broad Branch Road, NW, Washington DC, 20015, USA
[8]Centre for Science at Extreme Conditions and School of Physics and Astronomy, University of Edinburgh, EH9 3FD Edinburgh, United Kingdom
[9]Institute of Inorganic Chemistry, University of Cologne, Greinstrasse 6, 50939 Cologne, Germany
[10]European Synchrotron Radiation Facility, B.P.220, F-38043 Grenoble Cedex, France
*Corresponding author. Email: Yuqing.Yin@uni-bayreuth.de (Y.Y.)

Supplementary Methods

Sample preparation. BX90-type screw-driven diamond anvil cells (DACs)[1] equipped with 250 μm (DAC #1-#3) or 120 μm (DAC #4 and #5) culet diamond anvils were used (Table S1). One stack of halide (NaCl/NaBr/KCl/KBr) thin (2-5 μm) plate was loaded together with a drop of CCl_4 (DAC #1 and #2) or a piece of CBr_4 (DAC #3-#5) acts as the halogen source. Rhenium was used as the gasket material. NaCl, NaBr, KCl, and KBr powders were dried on a heating table at 220 °C for 48 h before loading to avoid any presence of water. The *in situ* pressure was measured using the first-order Raman mode of the stressed diamond anvils[2]. Double-sided sample laser-heating was performed at our home laboratory at the Bayerisches Geoinstitut[3] with carbon or bromine employed as the laser light absorber. Detailed information of pressure and the heating temperature can be found in Table S1.

X-ray diffraction. Synchrotron X-ray diffraction measurements of the compressed samples were performed at ID11 (λ = 0.2844 Å, beam size ~0.75 × 0.75 μm^2) and ID27 (λ = 0.3738 Å, beam size ~2.0 × 2.0 μm^2) of the EBS-ESRF and the P02.2 beamline (λ = 0.2907 Å, beam size ~2.0 × 2.0 μm^2) of PETRA III. In order to determine the sample position for single-crystal X-ray diffraction data acquisition, a full X-ray diffraction mapping of the pressure chamber was performed. The sample positions displaying the greatest number of single-crystal reflections belonging to the phases of interest were chosen, and step-scans of 0.5° from −36° to +36° ω were performed. The CrysAlis^{Pro} software[4] was utilized for the single-crystal data analysis. To calibrate the instrumental model in the CrysAlis^{Pro} software, *i.e.* the sample-to-detector distance, detector's origin, offsets of the goniometer angles, and rotation of both the X-ray beam and detector around the instrument axis, we used a single crystal of orthoenstatite [$(Mg_{1.93}Fe_{0.06})(Si_{1.93}Al_{0.06})O_6$, *Pbca* space group, a = 8.8117(2) Å, b = 5.1832(10) Å, and c = 18.2391(3) Å]. The DAFi program[5] was used for the search of reflections' groups belonging to individual single-crystal domains. The crystal structures were then solved and refined using the OLEX2[6] and JANA2006 software[7]. The crystallite sizes were estimated from X-ray maps. The crystallographic information is available in Tables S2-S10.

Raman spectroscopy. Raman spectroscopy measurements were performed with a LabRam spectrometer equipped with a ×50 Olympus objective. Sample excitation was accomplished using a continuous He-Ne laser (632.8 nm line) with a focused laser spot of about 2 μm in diameter. The Stokes Raman signal was collected in a backscattering geometry by a CCD coupled to an 1800 l/mm grating, allowing a spectral resolution of approximately 2 cm^{-1}. A laser power of about 4.6 mW incident on the DAC was employed. Raman spectra of CBr_4 were collected as a reference using a DAC loaded with pure CBr_4 (Figure S8).

Density functional theory calculations. First-principles calculations were performed using the framework of density functional theory (DFT) as implemented in the Vienna Ab initio Simulation Package (VASP)[8]. The Projector-Augmented-Wave (PAW) method[9-10] was used to expand the electronic wave functions in a plane wave basis. The Generalized Gradient Approximation (GGA) functional is used for calculating the exchange-correlation energies, as proposed by Perdew–Burke–Ernzerhof (PBE)[11]. The PAW potentials adapted from the VASP library with following valence configurations of 2*s*2*p*3*s* for Na, 3*s*3*p*4*s* for K, 3*s*3*p* for Cl, and 4*s*4*p* for Br were used. The plane-wave kinetic energy cutoff was set to 800 eV. We performed variable cell relaxations including lattice parameters and atomic positions on all synthesized experimental structures to optimize the atomic coordinates and the cell vectors until the total forces were smaller than 10^{-6} eV $Å^{-1}$ per atom using the conjugate-gradient (CG) algorithm. In geometry optimization, we used a Gamma centred k-mesh of 7x7x11 (for Na_4Cl_5, Na_4Br_5), 7x7x15 (for Na_2Cl_3), and 13x13x13 (for $NaCl_3$), respectively. To increase the accuracy of ground-state electron density and density of states (DOS), a denser Gamma centred k-mesh of 21x21x21 in case of $NaCl_3$ and 18x18x21 for Na_4Cl_5 (Na_4Br_5) were used considering the number of electronic bands twice than that of number of electrons in the respective systems. The tetrahedron smearing method with Blöchl corrections (ISMEAR = -5) were used for the pDOS and for the partial charge density around the Fermi energy.

The crystal structure, ELF, and charge density maps visualisation were made with the VESTA software[12]. The finite displacement method, as implemented in PHONOPY[13], was used to calculate harmonic phonon frequencies and phonon band structures. A supercell size of 2x2x3 in case of Na_4Cl_5 (Na_4Br_5), and 2x2x4 for Na_2Cl_3 were used with k-mesh size of 2x2x2 and 3x3x3 for the harmonic phonon calculations at 0 K. The finite-temperature phonon dispersion of Na_2Cl_3 (50 GPa) is using the temperature-dependent effective potential (TDEP) method[14]. The initial canonical configurations were created at thermalization temperature (300K) including the nuclear quantum effects in TDEP at a maximum phonon frequency of 16 THz for Na_2Cl_3 (50 GPa). Self-consistent iterations were performed to converge the second order interatomic force constants (FCs) by considering a cutoff radius of 6 Å in a 2x2x5 supercell containing 200 atoms. Crystal orbital Hamilton population (COHP) and crystal orbital bond index (COBI) analyses were performed using the LOBSTER package[15-19].

Supplementary Tables

Table S1. Summary of the experiments on high-pressure high-temperature synthesis in a diamond anvil cell.

DAC number	Starting materials	Pressure (GPa, ±1)	Measured temperature (K, ±200)	Reaction products
1	$NaCl + CCl_4 + C_{graphite}$	50	2100	*hP*18-Na_4Cl_5
		56	2200	*tP*10-Na_2Cl_3 *cP*8-$NaCl_3$
2	$KCl + CCl_4 + C_{graphite}$	41	2000	*cP*8-KCl_3
		50	2100	*hP*24-KCl_3
3	NaBr* + CBr_4	48	2000	*hP*18-Na_4Br_5
4	NaBr + CBr_4*	46	2200	*cP*8-$NaBr_3$ *oC*8-Br
		73	2300	*cP*8-$NaBr_3$ *hP*18-Na_4Br_5 *oC*8-Br
5	KBr + CBr_4*	80	2000	*cP*8-KBr_3

* The reagents marked with the star were put into the DACs in excess to explore the effect of different ratios of the starting materials on the reaction products.

Table S2. Crystal structure, data collection and refinement details of *cP*8-$NaCl_3$ at 50(1) and 56(1) GPa in comparison to the corresponding DFT-relaxed structure.

Crystal data			**DFT results**
Chemical formula	$NaCl_3$	$NaCl_3$	$NaCl_3$
M_r	129.34	129.34	
Crystal system, space group	Cubic, $Pm\bar{3}n$	Cubic, $Pm\bar{3}n$	Cubic, $Pm\bar{3}n$
Temperature (K)	293	293	
Pressure (GPa)	50(1)	56(1)	50
a (Å)	4.7070(3)	4.6737(9)	4.6743
V (Å^3)	104.29(2)	102.09(6)	102.1283
Z	2	2	
Radiation type	Synchrotron, λ = 0.2907 Å	Synchrotron, λ = 0.3738 Å	
μ (mm^{-1})	0.35	0.70	
Crystal size (mm)	0.001 × 0.001 × 0.001	0.001 × 0.001 × 0.001	
Data collection			
Diffractometer	LH@P02.2	ESRF ID27, EIGER2 X CdTe 9M detector	
Absorption correction	Multi-scan *CrysAlis PRO* 1.171.40.67a (Rigaku Oxford Diffraction, 2019) Empirical absorption correction using spherical harmonics, implemented in SCALE3 ABSPACK scaling algorithm.	Multi-scan *CrysAlis PRO* 1.171.40.67a (Rigaku Oxford Diffraction, 2019) Empirical absorption correction using spherical harmonics, implemented in SCALE3 ABSPACK scaling algorithm.	
T_{min}, T_{max}	0.786, 1	0.381, 1	
No. of measured, independent and observed [$I > 2\sigma(I)$] reflections	420, 72, 67	208, 58, 45	
R_{int}	0.104	0.056	
$(\sin\theta/\lambda)_{max}$ (Å^{-1})	0.908	0.920	
Refinement			
$R[F^2 > 2\sigma(F^2)]$, $wR(F^2)$, S	0.051, 0.126, 1.23	0.058, 0.186, 1.28	
No. of reflections	72	58	
No. of parameters	4	4	
$\Delta\rho_{max}$, $\Delta\rho_{min}$ (e Å^{-3})	1.00, -0.61	0.82, -0.76	
Crystal Structure			
Wyckoff Site	Na1: 2*a* Cl1: 6*d*	Na1: 2*a* Cl1: 6*d*	Na1: 2*a* Cl1: 6*d*
Fractional atomic coordinates (x y z)	Na1: 0 0 0 Cl1: 1/4 1/2 0	Na1: 0 0 0 Cl1: 1/4 1/2 0	Na1: 0 0 0 Cl1: 1/4 1/2 0
U_{iso} (Å^2)	Na1: 0.0137(7) Cl1: 0.0176(5)	Na1: 0.0224(12) Cl1: 0.0263(10)	

Table S3. Crystal structure, data collection and refinement details of *cP*8-KCl_3 at 41(1) and 50(1) GPa in comparison to the corresponding DFT-relaxed structure.

Crystal data			**DFT results**
Chemical formula	KCl_3	KCl_3	KCl_3
M_r	145.45	145.45	
Crystal system, space group	Cubic, $Pm\bar{3}n$	Cubic, $Pm\bar{3}n$	Cubic, $Pm\bar{3}n$
Temperature (K)	293	293	
Pressure (GPa)	41(1)	50(1)	42
a (Å)	4.9313(5)	4.8194(10)	4.9258
V (Å^3)	119.92(4)	111.94(7)	119.51717
Z	2	2	
Radiation type	Synchrotron, λ = 0.3738 Å	Synchrotron, λ = 0.3738 Å	
μ (mm^{-1})	0.84	0.90	
Crystal size (mm)	0.001 × 0.001 × 0.001	0.001 × 0.001 × 0.001	
Data collection			
Diffractometer	ESRF ID27, EIGER2 X CdTe 9M detector	ESRF ID27, EIGER2 X CdTe 9M detector	
Absorption correction	Multi-scan *CrysAlis PRO* 1.171.40.67a (Rigaku Oxford Diffraction, 2019) Empirical absorption correction using spherical harmonics, implemented in SCALE3 ABSPACK scaling algorithm.	Multi-scan *CrysAlis PRO* 1.171.40.67a (Rigaku Oxford Diffraction, 2019) Empirical absorption correction using spherical harmonics, implemented in SCALE3 ABSPACK scaling algorithm.	
T_{min}, T_{max}	0.235, 1	0.570, 1	
No. of measured, independent and observed [$I > 2\sigma(I)$] reflections	234, 58, 50	246, 68, 56	
R_{int}	0.016	0.052	
$(\sin\theta/\lambda)_{max}$ (Å^{-1})	0.890	0.892	
Refinement			
$R[F^2 > 2\sigma(F^2)]$, $wR(F^2)$, S	0.054, 0.150, 1.21	0.041, 0.103, 1.13	
No. of reflections	58	68	
No. of parameters	4	4	
$\Delta\rho_{max}$, $\Delta\rho_{min}$ (e Å^{-3})	1.02, -0.60	0.92, -0.97	
Crystal Structure			
Wyckoff Site	K1: 2*a* Cl1: 6*d*	K1: 2*a* Cl1: 6*d*	K1: 2*a* Cl1: 6*d*
Fractional atomic coordinates (x y z)	K1: 0 0 0 Cl1: 1/4 1/2 0	K1: 0 0 0 Cl1: 1/4 1/2 0	K1: 0 0 0 Cl1: 1/4 1/2 0
U_{iso} (Å^2)	K1: 0.0230(8) Cl1: 0.0336(8)	K1: 0.0154(5) Cl1: 0.0200(4)	

Table S4. Crystal structure, data collection and refinement details of *cP*8-KBr_3 at 80(1) GPa in comparison to the corresponding DFT-relaxed structure.

Crystal data		**DFT results**
Chemical formula	KBr_3	KBr_3
M_r	278.83	
Crystal system, space group	Cubic, $Pm\bar{3}n$	Cubic, $Pm\bar{3}n$
Temperature (K)	293	
Pressure (GPa)	80(1)	79.5
a (Å)	4.8898(3)	4.8898
V (Å^3)	116.92(2)	116.9158
Z	2	
Radiation type	Synchrotron, λ = 0.2844 Å	
μ (mm^{-1})	4.44	
Crystal size (mm)	0.001 × 0.001 × 0.001	
Data collection		
Diffractometer	ESRF ID11, Dectris Eiger2 X CdTe 4M	
Absorption correction	Multi-scan *CrysAlis PRO* 1.171.40.67a (Rigaku Oxford Diffraction, 2019) Empirical absorption correction using spherical harmonics, implemented in SCALE3 ABSPACK scaling algorithm.	
T_{min}, T_{max}	0.282, 1	
No. of measured, independent and observed [$I > 2\sigma(I)$] reflections	556, 80, 70	
R_{int}	0.026	
$(\sin\theta/\lambda)_{max}$ (Å^{-1})	0.903	
Refinement		
$R[F^2 > 2\sigma(F^2)]$, $wR(F^2)$, S	0.014, 0.036, 1.12	
No. of reflections	80	
No. of parameters	4	
$\Delta\rho_{max}$, $\Delta\rho_{min}$ (e Å^{-3})	2.06, -0.55	
Crystal Structure		
Wyckoff Site	K1: 2*a* Br1: 6*d*	K1: 2*a* Br1: 6*d*
Fractional atomic coordinates (x y z)	K1: 0 0 0 Br1: 1/4 1/2 0	K1: 0 0 0 Br1: 1/4 1/2 0
U_{iso} (Å^2)	K1: 0.0045(17) Br1: 0.0052(12)	

Table S5. Crystal structure, data collection and refinement details of *cP*8-$NaBr_{3-x}$ *with a partial occupancy of Br1 position at 46(1) and 73(1) GPa* in comparison to the corresponding DFT-relaxed structure.

Crystal data			**DFT results**
Chemical formula	$NaBr_{3-x}$	$NaBr_{3-x}$	$NaBr_3$
M_r	194.80	204.39	
Crystal system, space group	Cubic, $Pm\bar{3}n$	Cubic, $Pm\bar{3}n$	Cubic, $Pm\bar{3}n$
Temperature (K)	293	293	
Pressure (GPa)	46(1)	73(1)	80
a (Å)	5.0457(10)	4.7588(4)	4.7801
V (Å^3)	128.46(8)	107.77(3)	109.2225
Z	2	2	
Radiation type	Synchrotron, λ = 0.2907 Å	Synchrotron, λ = 0.2844 Å	
μ (mm^{-1})	3.01	3.55	
Crystal size (mm)	0.001 × 0.001 × 0.001	0.001 × 0.001 × 0.001	
Data collection			
Diffractometer	LH@P02.2	ESRF ID11, Dectris Eiger2 X CdTe 4M	
Absorption correction	Multi-scan *CrysAlis PRO* 1.171.40.67a (Rigaku Oxford Diffraction, 2019) Empirical absorption correction using spherical harmonics, implemented in SCALE3 ABSPACK scaling algorithm.	Multi-scan *CrysAlis PRO* 1.171.40.67a (Rigaku Oxford Diffraction, 2019) Empirical absorption correction using spherical harmonics, implemented in SCALE3 ABSPACK scaling algorithm.	
T_{min}, T_{max}	0.641, 1	0.606, 1	
No. of measured, independent and observed [$I > 2\sigma(I)$] reflections	190, 36, 29	586, 96, 79	
R_{int}	0.129	0.028	
$(\sin\theta/\lambda)_{max}$ (Å^{-1})	0.665	0.997	
Refinement			
$R[F^2 > 2\sigma(F^2)]$, $wR(F^2)$, S	0.083, 0.209, 1.21	0.026, 0.068, 1.13	
No. of reflections	36	96	
No. of parameters	5	5	
$\Delta\rho_{max}$, $\Delta\rho_{min}$ (e Å^{-3})	1.59, -1.59	1.57, -0.77	
Crystal Structure			
Wyckoff Site	Na1: 2*a* Br1: 6*d*	Na1: 2*a* Br1: 6*d*	Na1: 2*a* Br1: 6*d*
Fractional atomic coordinates (x y z), occupancy	Na1: 0 0 0, 1 Br1: 1/4 1/2 0, 0.72(8)	Na1: 0 0 0, 1 Br1: 1/4 1/2 0, 0.757(17)	Na1: 0 0 0, 1 Br1: 1/4 1/2 0, 1
U_{iso} (Å^2)	Na1: 0.021(8) Br1: 0.015(2)	Na1: 0.0099(8) Br1: 0.0104(18)	

Table S6. Comparison of agreement factors R_1 resulted from the *cP*8-$NaBr_{3-x}$ structure refinement using different models: with fully and partially occupied positions of Br atoms.

Pressure, (GPa, ±1)	No. of reflections	Fully occupied model		Partially occupied model	
		No. of parameters	R_1	No. of parameters	R_1
46	36	4	0.088	5	0.083
73	96	4	0.041	5	0.026

Table S7. Crystal structure, data collection and refinement details of *hP*24-KCl_3 at 41(1) and 50(1) GPa in comparison to the corresponding DFT-relaxed structure.

Crystal data			**DFT results**
Chemical formula	KCl_3	KCl_3	KCl_3
M_r	145.45	145.45	
Crystal system, space group	Trigonal, $P\bar{3}c1$	Trigonal, $P\bar{3}c1$	Trigonal, $P\bar{3}c1$
Temperature (K)	293	293	
Pressure (GPa)	41(1)	50(1)	40
a, c (Å)	6.991(3), 8.512(9)	6.7996(8), 8.3872(7)	6.9645, 8.5855
V (Å^3)	360.3(5)	335.83(8)	360.6429
Z	6	6	
Radiation type	Synchrotron, λ = 0.3738 Å	Synchrotron, λ = 0.3738 Å	
μ (mm^{-1})	0.84	0.90	
Crystal size (mm)	0.003 × 0.003 × 0.003	0.003 × 0.003 × 0.003	
Data collection			
Diffractometer	ESRF ID27, EIGER2 X CdTe 9M detector	ESRF ID27, EIGER2 X CdTe 9M detector	
Absorption correction	Multi-scan *CrysAlis PRO* 1.171.40.67a (Rigaku Oxford Diffraction, 2019) Empirical absorption correction using spherical harmonics, implemented in SCALE3 ABSPACK scaling algorithm.	Multi-scan *CrysAlis PRO* 1.171.40.67a (Rigaku Oxford Diffraction, 2019) Empirical absorption correction using spherical harmonics, implemented in SCALE3 ABSPACK scaling algorithm.	
T_{min}, T_{max}	0.635, 1	0.270, 1	
No. of measured, independent and observed [$I > 2\sigma(I)$] reflections	642, 274, 171	611, 331, 277	
R_{int}	0.039	0.013	
$(\sin\theta/\lambda)_{max}$ (Å^{-1})	0.779	0.904	
Refinement			
$R[F^2 > 2\sigma(F^2)]$, $wR(F^2)$, S	0.080, 0.245, 1.00	0.060, 0.156, 1.01	
No. of reflections	274	331	
No. of parameters	20	20	
$\Delta\rho_{max}$, $\Delta\rho_{min}$ (e Å^{-3})	1.77, -1.27	1.81, -1.06	
Crystal Structure			
Wyckoff Site	K1: 2*b* K2: 4*d* Cl1: 6*f* Cl2: 12*g*	K1: 2*b* K2: 4*d* Cl1: 6*f* Cl2: 12*g*	K1: 2*b* K2: 4*d* Cl1: 6*f* Cl2: 12*g*
Fractional atomic coordinates (x y z)	K1: 0 0 1/2 K2: 1/3 2/3 0.3459(3) Cl1: 0 0.2543(2) 3/4	K1: 0 0 1/2 K2: 1/3 2/3 0.34658(11) Cl1: 0 0.25474(12) 3/4	K1: 0 0 1/2 K2: 1/3 2/3 0.3515 Cl1: 0 0.2568 3/4

	Cl2: 0.3106(4) 0.4087(2) 0.5943(2)	Cl2: 0.31075(13) 0.40862(11) 0.59466(9)	Cl2: 0.3029 0.4067 0.5983
U_{iso} (Å^2)	K1: 0.0179(9) K2: 0.0177(8) Cl1: 0.0215(8) Cl2: 0.0213(7)	K1: 0.0114(3) K2: 0.0090(3) Cl1: 0.0124(3) Cl2: 0.0108(3)	

Table S8. Crystal structure, data collection and refinement details of *hP*18-Na_4Cl_5 at 50(1) and 56(1) GPa in comparison to the corresponding DFT-relaxed structure.

Crystal data			**DFT results**
Chemical formula	Na_4Cl_5	Na_4Cl_5	Na_4Cl_5
M_r	269.21	269.21	
Crystal system, space group	Hexagonal, $P6_3/mcm$	Hexagonal, $P6_3/mcm$	Hexagonal, $P6_3/mcm$
Temperature (K)	293	293	
Pressure (GPa)	50(1)	56(1)	58
a, c (Å)	7.329(2), 4.7757(18)	7.2603(15), 4.7524(12)	7.2751, 4.7476
V (Å^3)	222.14(17)	216.95(11)	217.6094
Z	2	2	
Radiation type	Synchrotron, λ = 0.2907 Å	Synchrotron, λ = 0.3738 Å	
μ (mm^{-1})	0.30	0.60	
Crystal size (mm)	0.003 × 0.003 × 0.003	0.003 × 0.003 × 0.003	
Data collection			
Diffractometer	LH@P02.2	ESRF ID27, EIGER2 X CdTe 9M detector	
Absorption correction	Multi-scan *CrysAlis PRO* 1.171.40.67a (Rigaku Oxford Diffraction, 2019) Empirical absorption correction using spherical harmonics, implemented in SCALE3 ABSPACK scaling algorithm.	Multi-scan *CrysAlis PRO* 1.171.40.67a (Rigaku Oxford Diffraction, 2019) Empirical absorption correction using spherical harmonics, implemented in SCALE3 ABSPACK scaling algorithm.	
T_{min}, T_{max}	0.581, 1	0.389, 1	
No. of measured, independent and observed [$I > 2\sigma(I)$] reflections	408, 133, 118	660, 193, 168	
R_{int}	0.073	0.022	
$(\sin\theta/\lambda)_{max}$ (Å^{-1})	0.714	0.933	
Refinement			
$R[F^2 > 2\sigma(F^2)]$, $wR(F^2)$, S	0.051, 0.116, 1.03	0.033, 0.086, 1.14	
No. of reflections	133	193	
No. of parameters	13	13	
$\Delta\rho_{max}$, $\Delta\rho_{min}$ (e Å^{-3})	0.70, -0.79	0.56, -0.42	
Crystal Structure			
Wyckoff Site	Na1: 2*b* Na2: 6*g* Cl1: 4*d* Cl2: 6*g*	Na1: 2*b* Na2: 6*g* Cl1: 4*d* Cl2: 6*g*	Na1: 2*b* Na2: 6*g* Cl1: 4*d* Cl2: 6*g*
Fractional atomic coordinates (x y z)	Na1: 0 0 0 Na2: 0 0.3821(4) 1/4 Cl1: 1/3 2/3 0 Cl2: 0 0.2764(3) 3/4	Na1: 0 0 0 Na2: 0 0.3823(2) 1/4 Cl1: 1/3 2/3 0 Cl2: 0 0.2771(12) 3/4	Na1: 0 0 0 Na2: 0 0.3819 1/4 Cl1: 1/3 2/3 0 Cl2: 0 0.2786 3/4

U_{iso} (Å^2)	Na1: 0.0130(11) Na2: 0.0097(7) Cl1: 0.0134(6) Cl2: 0.0082(5)	Na1: 0.0125(5) Na2: 0.0145(4) Cl1: 0.0175(3) Cl2: 0.0117(3)	

Table S9. Crystal structure, data collection and refinement details of *hP*18-Na_4Br_5 at 48(1) and 73(1) GPa in comparison to the corresponding DFT-relaxed structure.

Crystal data			**DFT results**
Chemical formula	Na_4Br_5	Na_4Br_5	Na_4Br_5
M_r	491.51	491.51	
Crystal system, space group	Hexagonal, $P6_3/mcm$	Hexagonal, $P6_3/mcm$	Hexagonal, $P6_3/mcm$
Temperature (K)	293	293	
Pressure (GPa)	48(1)	73(1)	80
a, c (Å)	7.6520(14), 5.1262(19)	7.3594(6), 4.9193(3)	7.3685, 4.9147
V (Å^3)	259.94(14)	230.74(4)	231.0877
Z	2	2	
Radiation type	Synchrotron, λ = 0.2907 Å	Synchrotron, λ = 0.2844 Å	
μ (mm^{-1})	3.47	3.68	
Crystal size (mm)	0.003 × 0.003 × 0.003	0.001 × 0.001 × 0.001	
Data collection			
Diffractometer	LH@P02.2	ESRF ID11, Dectris Eiger2 X CdTe 4M	
Absorption correction	Multi-scan *CrysAlis PRO* 1.171.40.67a (Rigaku Oxford Diffraction, 2019) Empirical absorption correction using spherical harmonics, implemented in SCALE3 ABSPACK scaling algorithm.	Multi-scan *CrysAlis PRO* 1.171.40.67a (Rigaku Oxford Diffraction, 2019) Empirical absorption correction using spherical harmonics, implemented in SCALE3 ABSPACK scaling algorithm.	
T_{min}, T_{max}	0.163, 1	0.219, 1	
No. of measured, independent and observed [$I > 2\sigma(I)$] reflections	612, 198, 162	1156, 248, 211	
R_{int}	0.051	0.037	
$(\sin\theta/\lambda)_{max}$ (Å^{-1})	0.877	0.875	
Refinement			
$R[F^2 > 2\sigma(F^2)]$, $wR(F^2)$, S	0.040, 0.100, 1.06	0.026, 0.061, 1.09	
No. of reflections	198	248	
No. of parameters	13	13	
$\Delta\rho_{max}$, $\Delta\rho_{min}$ (e Å^{-3})	1.25, -1.44	1.63, -1.38	
Crystal Structure			
Wyckoff Site	Na1: 2*b* Na2: 6*g* Br1: 4*d* Br2: 6*g*	Na1: 2*b* Na2: 6*g* Br1: 4*d* Br2: 6*g*	Na1: 2*b* Na2: 6*g* Br1: 4*d* Br2: 6*g*
Fractional atomic coordinates (x y z)	Na1: 0 0 0 Na2: 0 0.3820(5) 1/4 Br1: 1/3 2/3 0 Br2: 0 0.2754(10) 3/4	Na1: 0 0 0 Na2: 0 0.3820(3) 1/4 Br1: 1/3 2/3 0 Br2: 0 0.2766(8) 3/4	Na1: 0 0 0 Na2: 0 0.3815 1/4 Br1: 1/3 2/3 0 Br2: 0 0.2780 3/4

U_{iso} (Å^2)	Na1: 0.0136(13) Na2: 0.0127(7) Br1: 0.0116(3) Br2: 0.0102(3)	Na1: 0.0068(7) Na2: 0.0067(4) Br1: 0.0066(15) Br2: 0.00627(14)	

Table S10. Crystal structure, data collection and refinement details of *tP*10-Na_2Cl_3 at 50(1) and 56(1) GPa in comparison to the corresponding DFT-relaxed structure.

Crystal data			**DFT results**
Chemical formula	Na_2Cl_3	Na_2Cl_3	Na_2Cl_3
M_r	152.33	152.33	
Crystal system, space group	Tetragonal, *P*4/*mbm*	Tetragonal, *P*4/*mbm*	Tetragonal, *P*4/*mbm*
Temperature (K)	293	293	
Pressure (GPa)	50(1)	56(1)	47
a, c (Å)	6.569(2), 3.0758(16)	6.533(3), 3.0363(11)	6.6055, 2.9732
V (Å^3)	132.75(11)	129.58(12)	129.7269
Z	2	2	
Radiation type	Synchrotron, λ = 0.2907 Å	Synchrotron, λ = 0.3738 Å	
μ (mm^{-1})	0.30	0.58	
Crystal size (mm)	0.003 × 0.003 × 0.003	0.001 × 0.001 × 0.001	
Data collection			
Diffractometer	LH@P02.2	ESRF ID27, EIGER2 X CdTe 9M detector	
Absorption correction	Multi-scan *CrysAlis PRO* 1.171.40.67a (Rigaku Oxford Diffraction, 2019) Empirical absorption correction using spherical harmonics, implemented in SCALE3 ABSPACK scaling algorithm.	Multi-scan *CrysAlis PRO* 1.171.40.67a (Rigaku Oxford Diffraction, 2019) Empirical absorption correction using spherical harmonics, implemented in SCALE3 ABSPACK scaling algorithm.	
T_{min}, T_{max}	0.508, 1	0.747, 1	
No. of measured, independent and observed [$I > 2\sigma(I)$] reflections	238, 92, 77	306, 98, 79	
R_{int}	0.075	0.044	
$(\sin\theta/\lambda)_{max}$ (Å^{-1})	0.655	0.714	
Refinement			
$R[F^2 > 2\sigma(F^2)]$, $wR(F^2)$, S	0.046, 0.118, 1.12	0.043, 0.106, 1.17	
No. of reflections	92	98	
No. of parameters	11	11	
$\Delta\rho_{max}$, $\Delta\rho_{min}$ (e Å^{-3})	1.04, -0.69	0.52, -0.84	
Crystal Structure			
Wyckoff Site	Na1: 4*g* Cl1: 2*a* Cl2: 4*h*	Na1: 4*g* Cl1: 2*a* Cl2: 4*h*	Na1: 4*g* Cl1: 2*a* Cl2: 4*h*
Fractional atomic coordinates (x y z)	Na1: 0.1425(4) 0.3575(4) 0 Cl1: 0 0 0 Cl2: 0.3443(2) 0.1557(2) 1/2	Na1: 0.3583(4) 0.1417(4) 0.0000 Cl1: 0 0 0 Cl2: 0.1563(2) 0.3437(2) 1/2	Na1: 0.3587 0.1413 0 Cl1: 0 0 0 Cl2: 0.1586 0.3414 1/2

U_{iso} (Å^2)	Na1: 0.0104(10) Cl1: 0.0126(9) Cl2: 0.0099(8)	Na1: 0.0193(9) Cl1: 0.0199(7) Cl2: 0.0180(6)	

Table S11. The parameters of the third order Birch-Murnaghan equations of states (BM3 EOSes) used to fit the theoretical P-V data for all synthesized phases.

Compound	Space group	Bulk modulus K_0 (GPa)	K_0'	V_0 (Å^3)
*hP*18-Na_4Cl_5	*P*6$_3$/*mcm*	27.3(9)	4.42(4)	388.0(2)
*tP*10-Na_2Cl_3	*P*4/*mbm*	25.7(8)	4.41(4)	223.0(12)
*cP*8-$NaCl_3$	$Pm\bar{3}n$	34.9(9)	4.29(3)	167.0(6)
*cP*8-KCl_3	$Pm\bar{3}n$	27.6(9)	4.62(4)	194.4(10)
*hP*24-KCl_3	$P\bar{3}c1$	11.2(8)	4.86(6)	708.0(9)
*hP*18-Na_4Br_5	*P*6$_3$/*mcm*	22.9(9)	4.45(4)	467.0(3)
*cP*8-$NaBr_3$	$Pm\bar{3}n$	28.4(10)	4.46(4)	208.4(12)
*cP*8-KBr_3	$Pm\bar{3}n$	25.3(8)	4.47(4)	229.4(13)

Table S12. Calculated Löwdin and Bader charge for specified atoms in B2-NaCl, *cP*8 $NaCl_3$ and $NaBr_3$, and *hP*18 Na_4Cl_5 and Na_4Br_5 at 50 GPa, and *tP*10-Na_2Cl_3 at 100 GPa.

Compound	Atom name	Wyckoff Site	Löwdin charge	Bader charge
B2-NaCl[a]	Na1	1*a*	0.66	0.82
	Cl1	1*b*	-0.66	-0.82
*cP*8-$NaCl_3$	Na1	2*a*	0.58	0.84
	Cl1	6*d*	-0.19	-0.28
*cP*8-$NaBr_3$	Na1	2*a*	0.53	0.83
	Br1	6*d*	-0.18	-0.28
*hP*18-Na_4Cl_5	Na1	2*b*	0.64	0.80
	Na2	6*g*	0.63	0.84
	Cl1	4*d*	-0.30	-0.43
	Cl2	6*g*	-0.65	-0.82
*hP*18-Na_4Br_5	Na1	2*b*	0.57	0.78
	Na2	6*g*	0.58	0.81
	Br1	4*d*	-0.27	-0.42
	Br2	6*g*	-0.59	-0.79
*tP*10-Na_2Cl_3	Na1	4*g*	0.61	0.80
	Cl1	2*a*	-0.28	-0.35
	Cl2	4*h*	-0.47	-0.62

[a] The calculated Löwdin and Bader charge for specified atoms in B2-NaCl is presented as a reference.

Table S13. Calculated integrated COBI and COHP (ICOBI and ICOHP) values between specified atoms in B2-NaCl, *cP*8 $NaCl_3$ and $NaBr_3$, and *hP*18 Na_4Cl_5 and Na_4Br_5 at 50 GPa, and *tP*10-Na_2Cl_3 at 100 GPa.

Compound	Atom 1[a]	Atom 2[a]	Distance ($d_{atom1-atom2}$)[b], Å	ICOBI (at) E_F	-ICOHP (at) E_F
B2-NaCl[c]	Na1	Na1	2.925	0.018	0.328
	Na1	Cl1	2.533	0.057	0.558
	Cl1	Cl1	2.925	0.014	0.017
*cP*8-$NaCl_3$	Na1	Cl1	2.613	0.047	0.510
	Cl1	Cl1	2.337	0.285	1.476
*cP*8-$NaBr_3$	Na1	Br1	2.778	0.051	0.509
	Br1	Br1	2.485	0.282	1.543
*hP*18-Na_4Cl_5	Na1	Na1	2.402	0.031	0.722
	Na2	Na2	2.966	0.019	0.384
	Na1	Cl2	2.375	0.077	0.742
	Na2	Cl1	2.593	0.044	0.480
	Na2	Cl2	2.504, 2.520, 2.521	0.068, 0.063, 0.063	0.636, 0.581, 0.594
	Cl1	Cl1	2.402	0.197	1.056
	Cl1	Cl2	2.939	0.009	0.017
*hP*18-Na_4Br_5	Na1	Na1	2.554	0.030	0.616
	Na1	Br2	2.481	0.086	0.803
	Na2	Br1	2.716	0.049	0.508
	Na2	Br2	2.622, 2.625, 2.677	0.072, 0.073, 0.063	0.628, 0.650, 0.569
	Br1	Br1	2.554	0.195	1.109
*tP*10-Na_2Cl_3	Na1	Na1	2.800	0.022	0.439
	Na1	Cl1	2.401	0.052	0.630
	Na1	Cl2	2.245, 2.322	0.077, 0.057	0.852, 0.632
	Cl1	Cl1	2.800	0.074	0.249
	Cl1	Cl2	2.699	0.032	0.176
	Cl2	Cl2	2.800, 2.859	0.027, 0.022	0.121, 0.093

[a] The Wyckoff Site information of atom 1 and atom 2 can be found in Table S12. [b] Only distances from 1 Å to 3 Å were considered. [c] The calculated ICOBI and ICOHP between specified atoms in B2-NaCl is presented as a reference.

Supplementary Figures

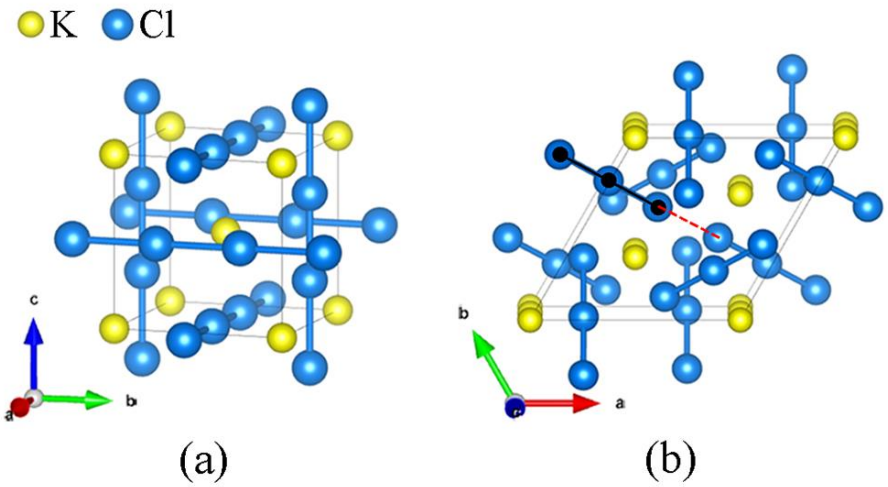

Figure S1. The structures of two high-pressure polymorphs of KCl_3 synthesised at 41 GPa and 2000 K. (a) *cP*8-KCl_3 (space group $Pm\bar{3}n$), which is isostructural with *cP*8-$NaCl_3$, *cP*8-KBr_3, and *cP*8-$NaBr_{3-x}$ (see text); interatomic Cl1-Cl1 distances in the linear chains are equal to 2.4657(3) Å; (b) *hP*24-KCl_3 (space group $P\bar{3}c1$), intramolecular Cl1-Cl2 distances in the trichloride anion (black lines) and intermolecular Cl2-Cl2 (red dashed line) distances are equal to 2.301(3) and 2.800(5) Å, respectively. Yellow balls are K atoms, blue balls - Cl atoms.

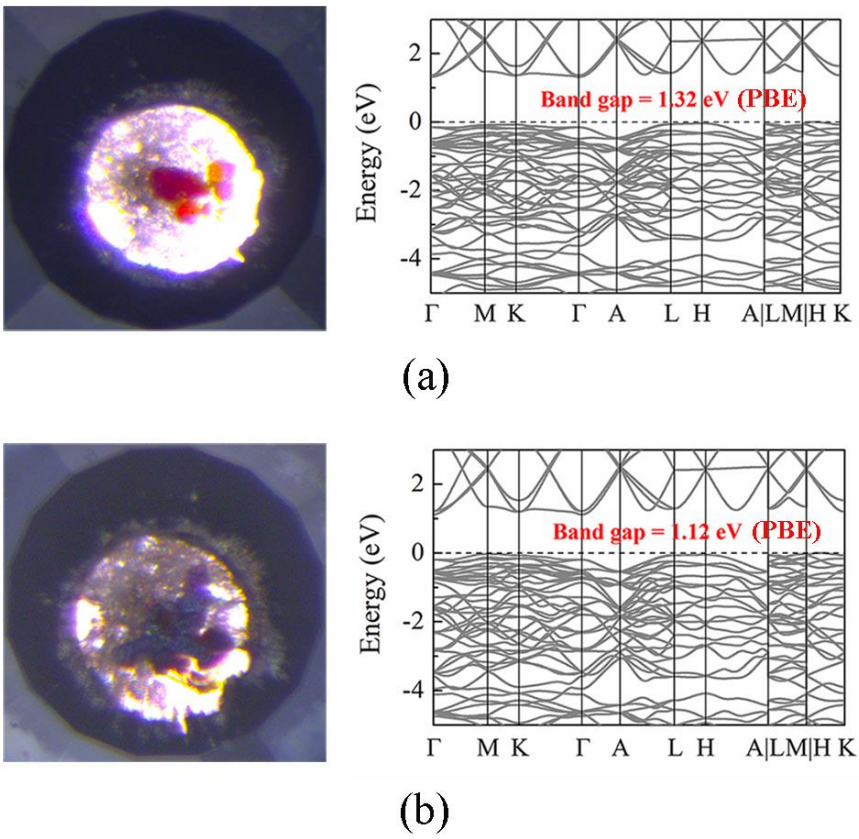

Figure S2. Images of a sample of *hP*24-KCl_3 in the pressure chamber of DAC #2 taken under an optical microscope and calculated band structures of *hP*24-KCl_3 at corresponding pressures. (a) 41 GPa; (b) 50 GPa. The Fermi energy level was set to 0 eV. The darker color of the sample at higher pressure agrees well with closing the band gap.

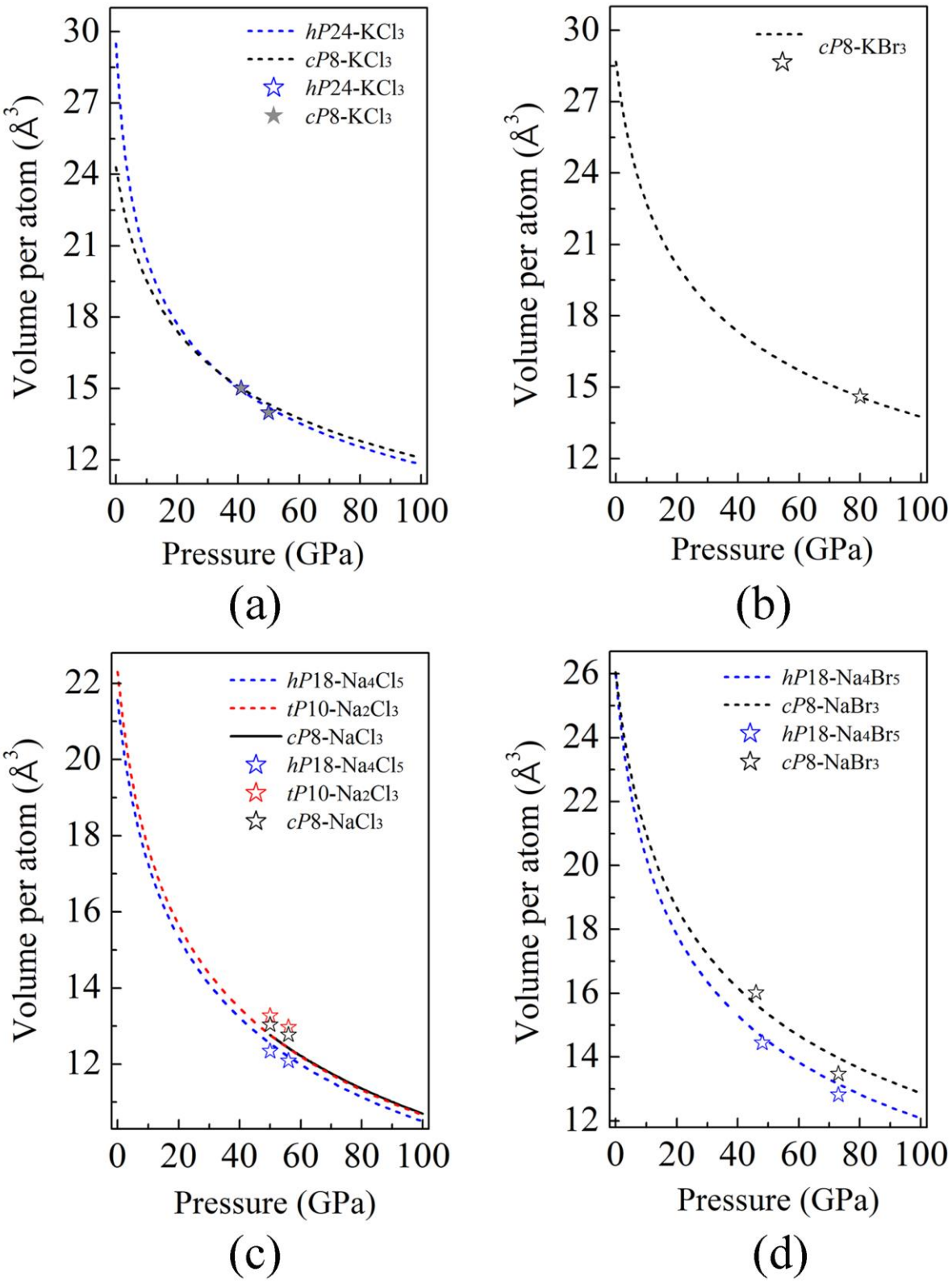

Figure S3. The pressure dependences of the volume per atom based on the pressure-volume relations from our DFT calculations in comparison with experimental data for (a) *hP*24-KCl_3 and *cP*8-KCl_3; (b) *cP*8-KBr_3; (c) *cP*8-$NaCl_3$, *tP*10-Na_2Cl_3, and *hP*18-Na_4Cl_5; (d) *cP*8-$NaBr_3$ and *hP*18-Na_4Br_5. Dashed lines represent DFT-calculated pressure for given volume fitted by BM3 EOSes. Stars of different colors represent experimental values.

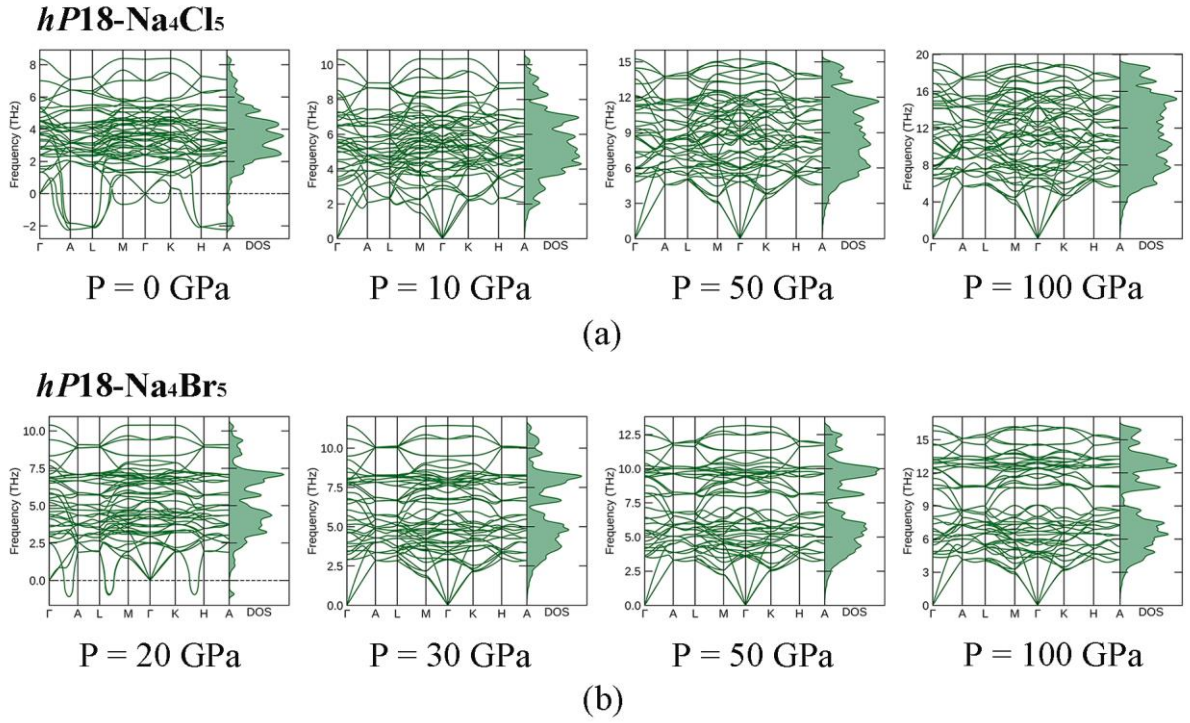

Figure S4. Phonon dispersion curves calculated at various pressures along high-symmetry directions in the Brillouin zone and resulting phonon density of states for (a) *hP*18-Na_4Cl_5 and (b) *hP*18-Na_4Br_5.

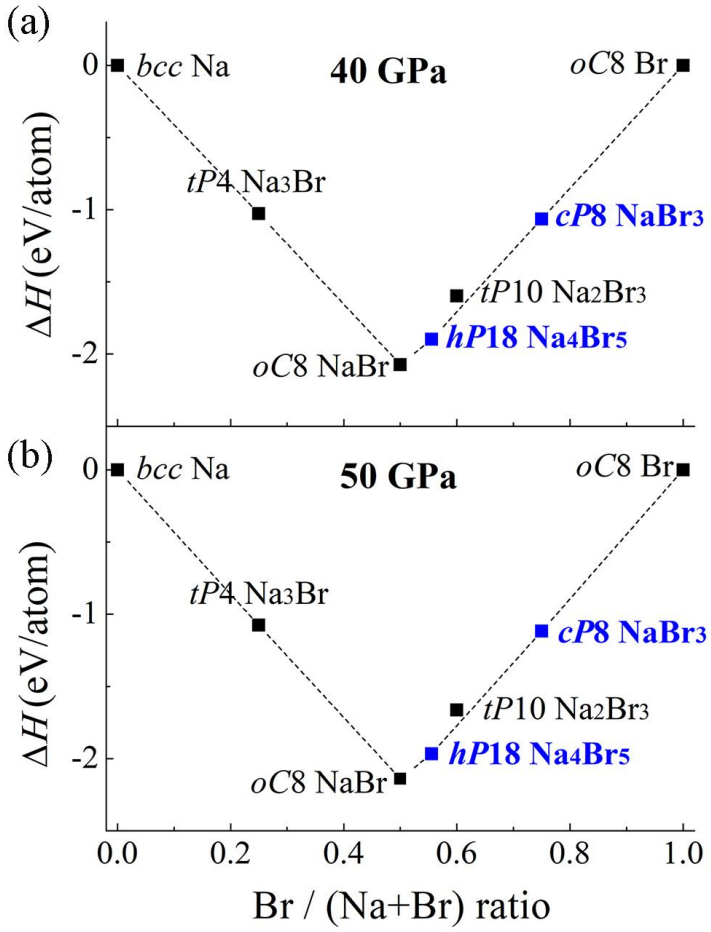

Figure S5. Convex hull diagrams for the Na-Br system at different pressures. (a) 40 GPa; (b) 50 GPa. The compounds synthesized in this work are highlighted in blue bold font.

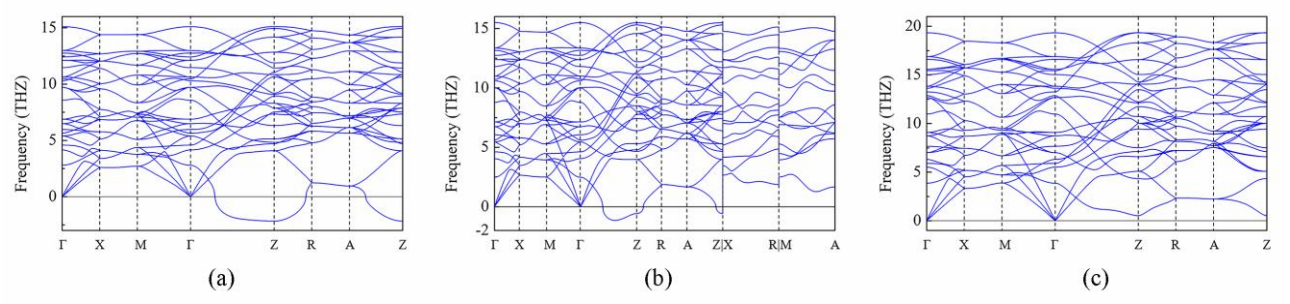

Figure S6. Phonon dispersion curves for *tP*10-Na_2Cl_3 calculated at (a) 0 K and (b) 300 K at 50 GPa, and (c) 0K at 100 GPa along high-symmetry directions in the Brillouin zone.

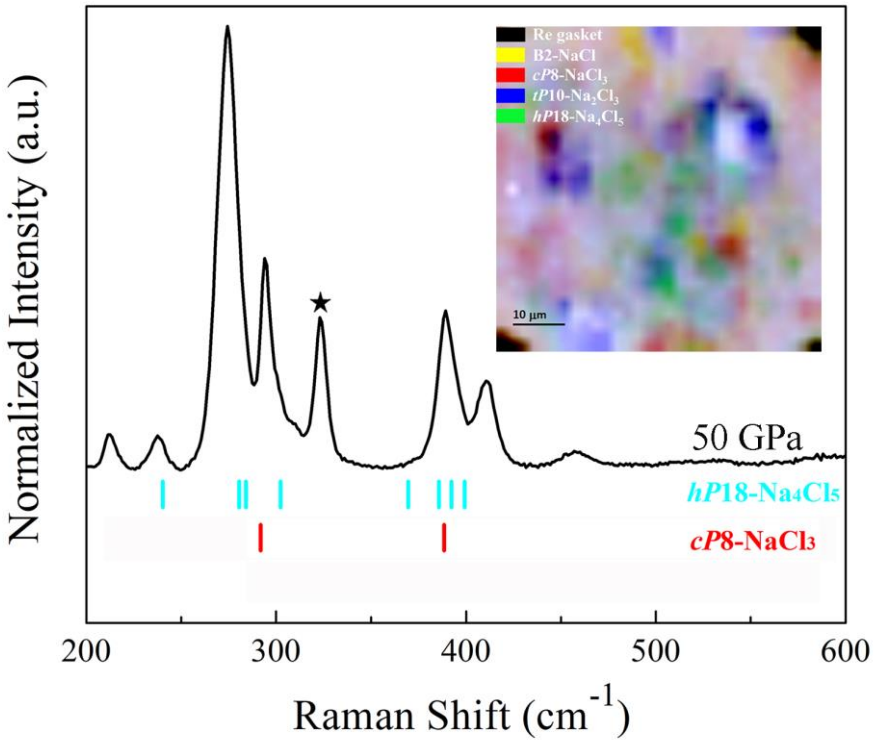

Figure S7. Raman spectrum taken from the sample in DAC #1 at 50 GPa and room temperature after laser heating of NaCl + CCl_4 + $C_{graphite}$ mixture to ~2000 K. The phase composition of this sample was determined using XRD mapping of the whole sample chamber, which revealed an uneven distribution of B2-NaCl, *hP*18-Na_4Cl_5, *tP*10-Na_2Cl_3, and *cP*8-$NaCl_3$ phases, formed as a result of chemical reactions (see inset). Vertical bars correspond to the positions of the Brillouin-zone-center optical phonons for *cP*8-$NaCl_3$ (red) and *hP*18-Na_4Cl_5 (bright cyan) computed in this work. Since harmonic phonon dispersion curves of *tP*10-Na_2Cl_3 calculated at 50 GPa show imaginary modes, we were not able to calculate its positions of the Brillouin-zone-center optical phonons. Raman peak at 323 cm^{-1} (marked with an asterisk) can be assigned to the A_g mode of *oC*8 chlorine[20-21]. We conclude that all these phases may contribute to the Raman spectrum observed (black line).

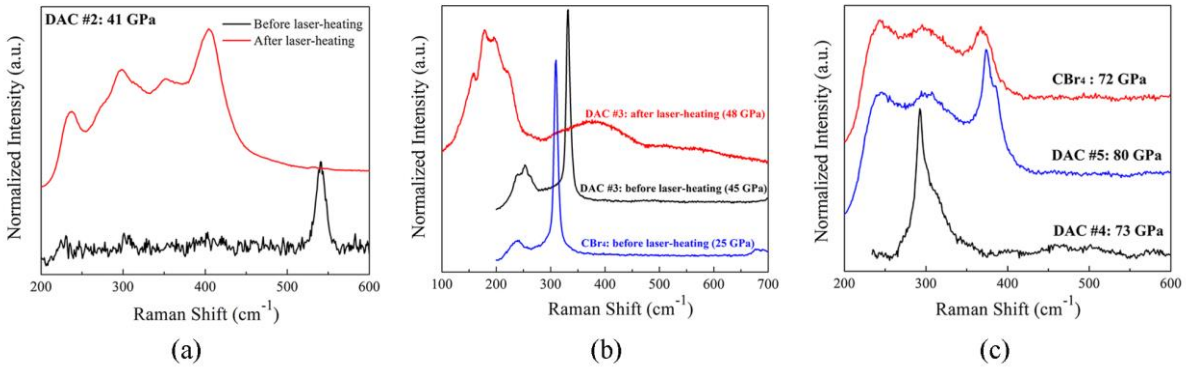

Figure S8. Raman spectra taken from samples in DACs #2, #3, #4, and #5 at different pressures before and after laser heating. (a) DAC #2: before heating of KCl + CCl_4 + $C_{graphite}$ mixture (black line) and after heating (red line) at 41 GPa; the peak at 540 cm^{-1} before heating can be assigned to CCl_4[22]; after heating *hP*24-KCl_3 and *cP*8-KCl_3 phases were detected in this DAC using XRD; (b) DAC #3: before heating of CBr_4 + NaBr mixture (with NaBr in excess) (black line) at 45 GPa and after heating (red line) at 48 GPa, and a DAC loaded with pure CBr_4 (at 25 GPa before heating for reference, blue line); the peaks before heating of DAC #3 (at ~253 and 331 cm^{-1}) can be assigned to CBr_4; after heating *hP*18-Na_4Br_5 phase was detected in this DAC using XRD; (c) DAC #4 (NaBr+CBr_4 at 73 GPa after heating, black line), DAC #5 (KBr + CBr_4 at 80 GPa after heating, blue line), and a DAC loaded with pure CBr_4 (at 72 GPa after heating for reference, red line); *cP*8-$NaBr_3$ and *hP*18-Na_4Br_5 phases were detected in DAC #4 and *cP*8-KBr_3 was detected in DAC #5 after heating, but the signals of these reaction products are unable to detect due to strong signals from CBr_4 (from ~230 to 390 cm^{-1}).

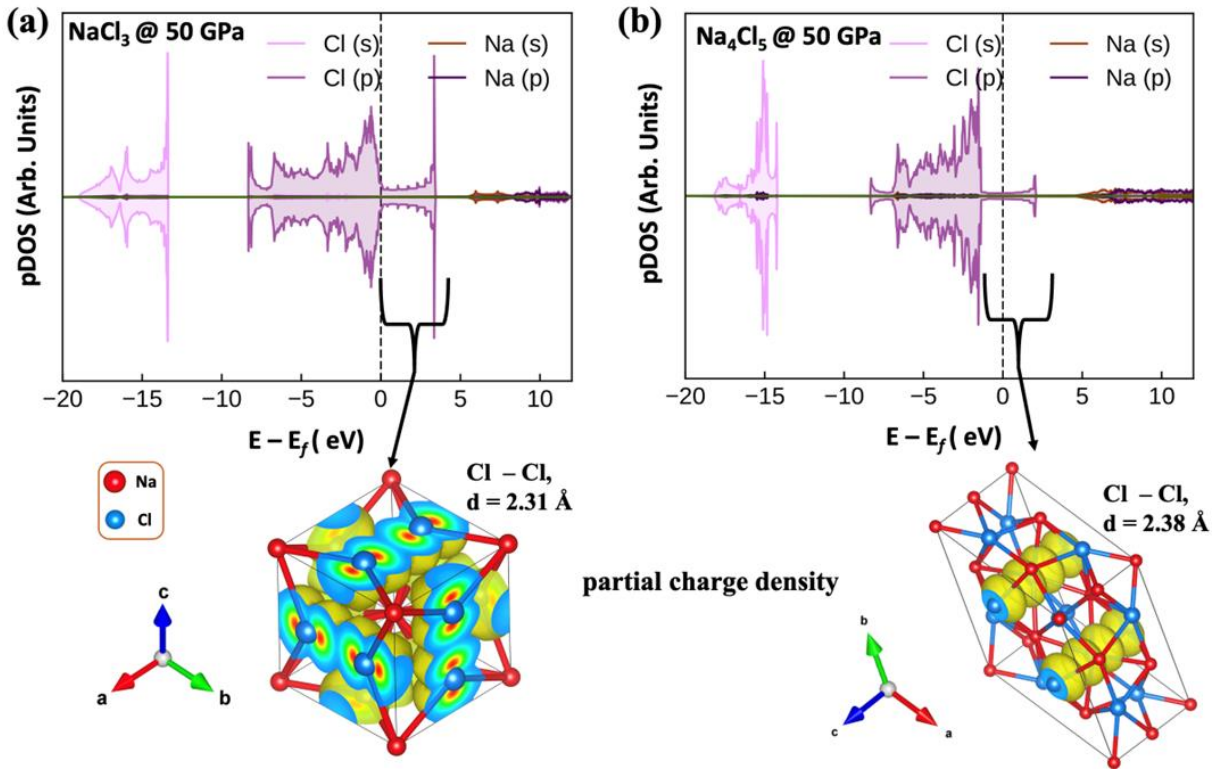

Figure S9. (a) (b) Projected electronic density of states (pDOS), and the corresponding partial electronic density of quasi-1D states near the Fermi energy for *cP*8-$NaCl_3$ and *hP*18-Na_4Cl_5 at 50 GPa. The shortest Cl-Cl bond distance is shown in the case of *hP*18-Na_4Cl_5 (50 GPa) on which the quasi-1D electron density lies along the *c*-axis.

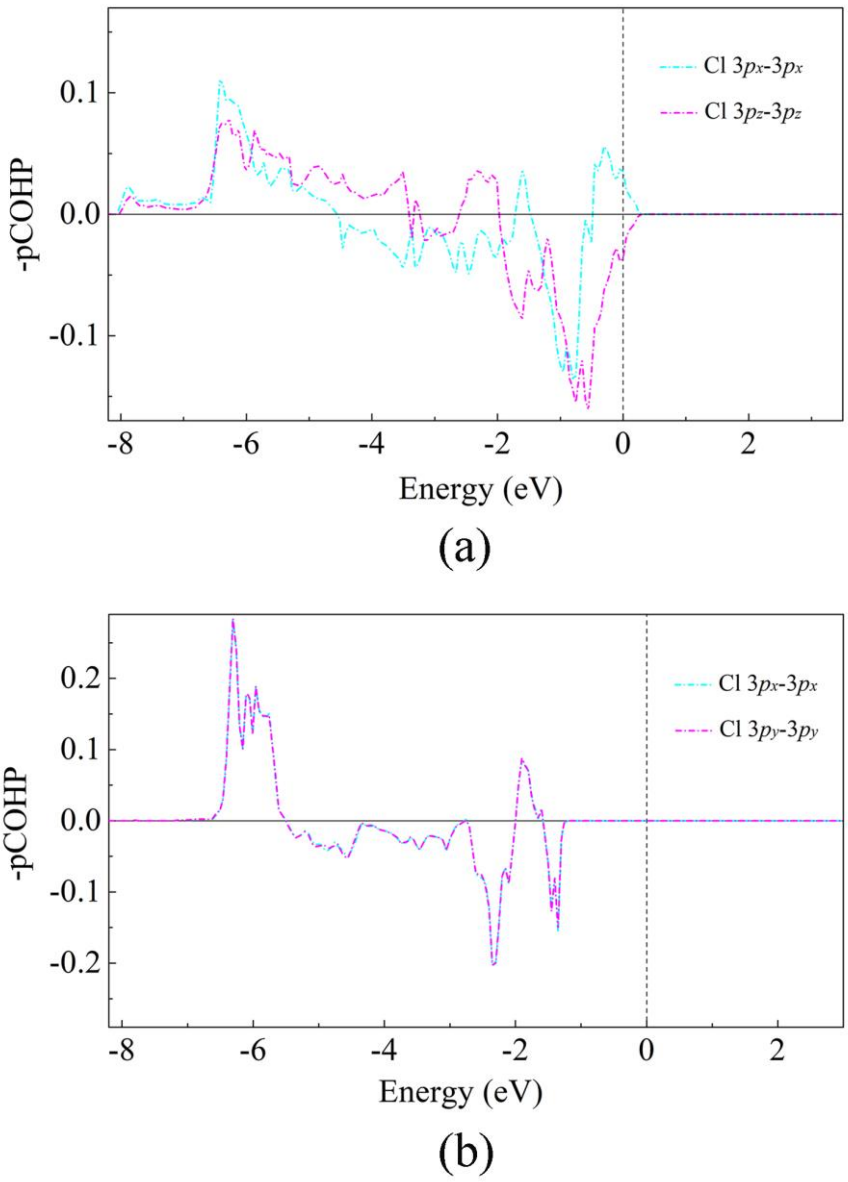

Figure S10. Detailed plot of the -PCOHP curves showing the π and π* features for (a) *cP*8-$NaCl_3$ (Cl $3p_x$-$3p_x$ and Cl $3p_z$-$3p_z$) and (b) *hP*18-Na_4Cl_5 (Cl $3p_x$-$3p_x$ and Cl $3p_y$-$3p_y$). The vertical dashed line indicates the Fermi energy.

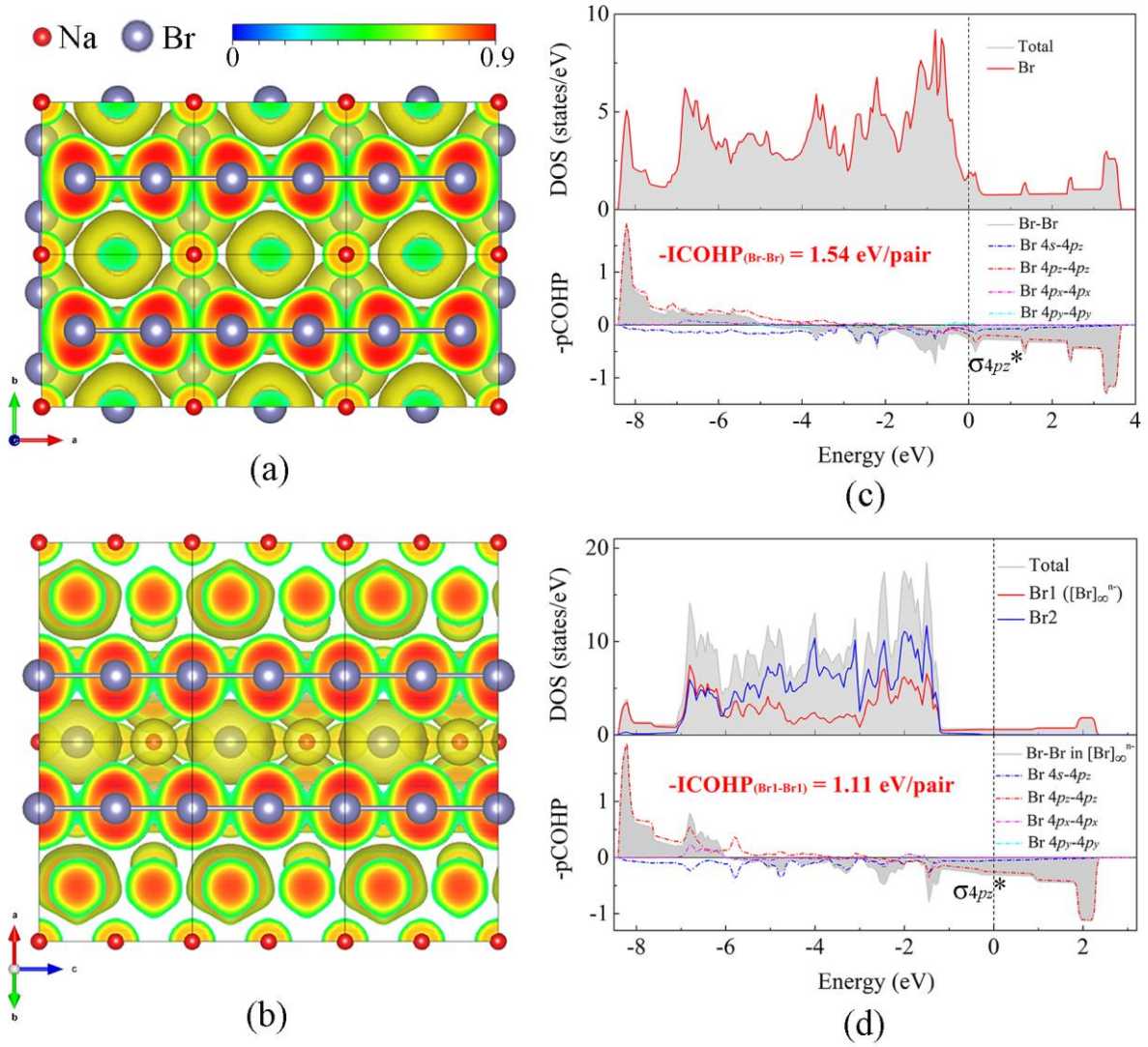

Figure S11. Calculated properties of *cP*8-$NaBr_3$ and *hP*18-Na_4Br_5 at 50 GPa. (a) Electron localization function (ELF) calculated in (001) plane for *cP*8-$NaBr_3$ and (b) in (110) plane for *hP*18-Na_4Br_5. The isosurfaces value is set as 0.3. Na and Br atoms are shown in red and purple colors. Calculated TDOS and PDOS curves for (c) *cP*8-$NaBr_3$ and (d) *hP*18-Na_4Br_5 along with the -pCOHP and -ICOHP for the Br-Br bond in the linear $[Br]_\infty^{n-}$ chains. The vertical dashed line indicates the Fermi energy.

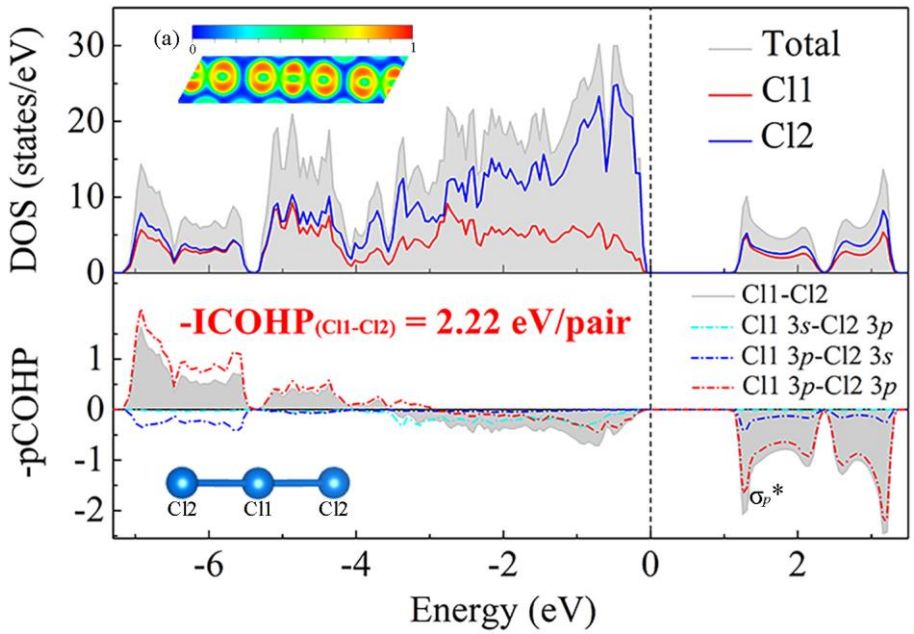

Figure S12. Calculated TDOS and PDOS curves of *hP*24-KCl_3 together with the -pCOHP and -ICOHP of the Cl1-Cl2 bond in the isolated $[Cl_3]^-$ molecules. The vertical dashed line indicates the Fermi energy. Cl1 represents the middle Cl atom and Cl2 represents the terminal Cl atom. The insert (a) shows the 2D ELF map of *hP*24-KCl_3 at 50 GPa cut along the $[Cl_3]^-$ planes, which is similar to the ELF distribution of XeF_2 (see ELF of XeF_2 at 50 GPa published by Miao[23]).

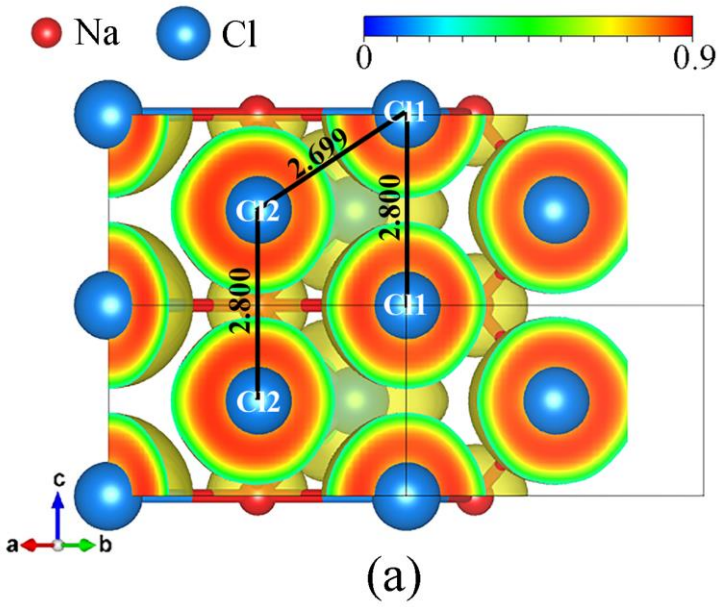

(a)

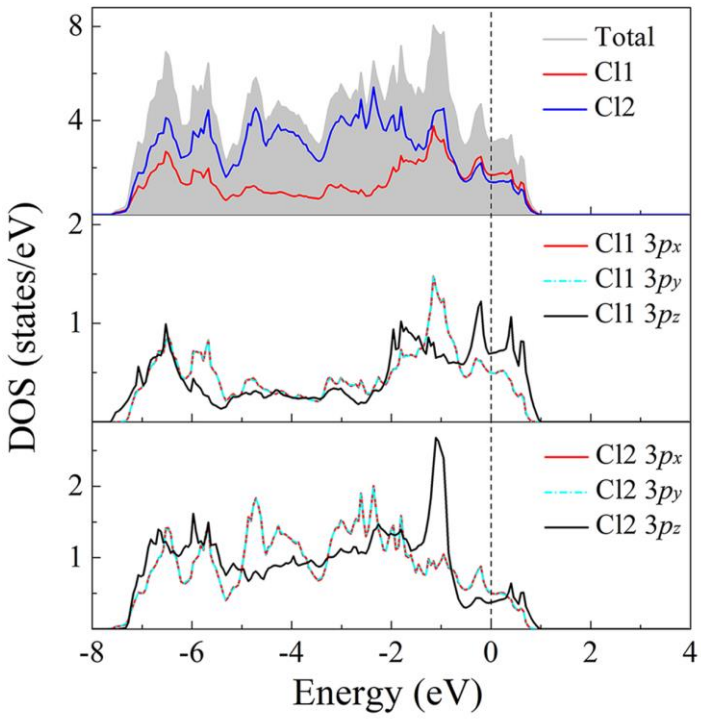

(b)

Figure S13. (a) ELF of *tP*10-Na_2Cl_3 cut along the section plane of the first neighboring Cl atoms (Cl1-Cl2) calculated at 100 GPa. Important Cl-Cl distances (Å) are presented. The isosurfaces value is set as 0.3. Na and Cl atoms are shown in red and blue colors. (b) The TDOS and PDOS curves, and Cl-3*p* orbitals in *tP*10-Na_2Cl_3 at 100 GPa. The vertical dashed line indicates the Fermi energy.

Supplementary References

1. Kantor, I.; Prakapenka, V.; Kantor, A.; Dera, P.; Kurnosov, A.; Sinogeikin, S.; Dubrovinskaia, N.; Dubrovinsky, L., BX90: a new diamond anvil cell design for X-ray diffraction and optical measurements. *Rev. Sci. Instrum.* **2012,** *83* (12), 125102.
2. Akahama, Y.; Kawamura, H., Pressure calibration of diamond anvil Raman gauge to 310GPa. *J. Appl. Phys.* **2006,** *100* (4), 043516.
3. Fedotenko, T.; Dubrovinsky, L.; Aprilis, G.; Koemets, E.; Snigirev, A.; Snigireva, I.; Barannikov, A.; Ershov, P.; Cova, F.; Hanfland, M., Laser heating setup for diamond anvil cells for in situ synchrotron and in house high and ultra-high pressure studies. *Rev. Sci. Instrum.* **2019,** *90* (10), 104501.
4. Rigaku Oxford Diffraction Ltd. *Rigaku OD and CryAlis PRO* **2018**.
5. Aslandukov, A.; Aslandukov, M.; Dubrovinskaia, N.; Dubrovinsky, L., Domain Auto Finder (DAFi) program: the analysis of single-crystal X-ray diffraction data from polycrystalline samples. *J. Appl. Crystallogr.* **2022,** *55* (Pt 5), 1383-1391.
6. Dolomanov, O. V.; Bourhis, L. J.; Gildea, R. J.; Howard, J. A. K.; Puschmann, H., OLEX2: a complete structure solution, refinement and analysis program. *J. Appl. Crystallogr.* **2009,** *42* (2), 339-341.
7. Petříček, V.; Dušek, M.; Palatinus, L., Crystallographic Computing System JANA2006: General features. *Z KRIST-CRYST MATER* **2014,** *229* (5), 345-352.
8. Kresse, G.; Furthmuller, J., Efficiency of ab-initio total energy calculations for metals and semiconductors using a plane-wave basis set. *Comput. Mater. Sci.* **1996,** *6* (1), 15-50.
9. Blochl, P. E., Projector augmented-wave method. *Phys. Rev., B Condens. Matter* **1994,** *50* (24), 17953-17979.
10. Kresse, G.; Joubert, D., From ultrasoft pseudopotentials to the projector augmented-wave method. *Phys Rev B* **1999,** *59* (3), 1758-1775.
11. Perdew, J. P.; Burke, K.; Ernzerhof, M., Generalized Gradient Approximation Made Simple. *Phys. Rev. Lett.* **1996,** *77* (18), 3865-3868.
12. Momma, K.; Izumi, F., VESTA: a three-dimensional visualization system for electronic and structural analysis. *J. Appl. Crystallogr.* **2008,** *41* (3), 653-658.
13. Togo, A.; Oba, F.; Tanaka, I., First-principles calculations of the ferroelastic transition between rutile-type and CaCl2-type SiO2 at high pressures. *Phys Rev B* **2008,** *78* (13), 134106.
14. Hellman, O.; Abrikosov, I.; Simak, S., Lattice dynamics of anharmonic solids from first principles. *Physical Review B* **2011,** *84* (18), 180301.
15. Dronskowski, R.; Bloechl, P. E., Crystal orbital Hamilton populations (COHP): energy-resolved visualization of chemical bonding in solids based on density-functional calculations. *The Journal of Physical Chemistry* **2002,** *97* (33), 8617-8624.
16. Müller, P. C.; Ertural, C.; Hempelmann, J.; Dronskowski, R., Crystal Orbital Bond Index: Covalent Bond Orders in Solids. *The Journal of Physical Chemistry C* **2021,** *125* (14), 7959-7970.
17. Deringer, V. L.; Tchougreeff, A. L.; Dronskowski, R., Crystal orbital Hamilton population (COHP) analysis as projected from plane-wave basis sets. *J. Phys. Chem. A* **2011,** *115* (21), 5461-6.
18. Maintz, S.; Deringer, V. L.; Tchougreeff, A. L.; Dronskowski, R., Analytic projection from plane-wave and PAW wavefunctions and application to chemical-bonding analysis in solids. *J. Comput. Chem.* **2013,** *34* (29), 2557-67.
19. Maintz, S.; Deringer, V. L.; Tchougreeff, A. L.; Dronskowski, R., LOBSTER: A tool to extract chemical bonding from plane-wave based DFT. *J. Comput. Chem.* **2016,** *37* (11), 1030-5.
20. Johannsen, P. G.; Holzapfel, W. B., Effect of pressure on Raman spectra of solid chlorine. *Journal of Physics C: Solid State Physics* **1983,** *16* (33), L1177-L1179.
21. Dalladay-Simpson, P.; Binns, J.; Pena-Alvarez, M.; Donnelly, M. E.; Greenberg, E.; Prakapenka, V.; Chen, X. J.; Gregoryanz, E.; Howie, R. T., Band gap closure, incommensurability and molecular dissociation of dense chlorine. *Nat Commun* **2019,** *10* (1), 1134.

22. Pravica, M.; Sneed, D.; Wang, Y.; Smith, Q.; Subrahmanyam, G., Carbon tetrachloride under extreme conditions. *J. Chem. Phys.* **2014,** *140* (19), 194503.
23. Miao, M. S., Caesium in high oxidation states and as a p-block element. *Nat Chem* **2013,** *5* (10), 846-52.